18

Laser-Plasma Extreme Ultraviolet Source Incorporating a Cryogenic Xe Target

Sho Amano
University of Hyogo
Laboratory of Advanced Science and Technology for Industry (LASTI)
Japan

1. Introduction

Optical lithography is a core technique used in the industrial mass production of semiconductor memory chips. To increase the memory size per chip, shorter wavelength light is required for the light source. ArF excimer laser light (193 nm) is used at present and extreme ultraviolet (EUV) light (13.5 nm) is proposed in next-generation optical lithography. There is currently worldwide research and development for lithography using EUV light (Bakshi, 2005). EUV lithography (EUVL) was first demonstrated by Kinoshita et al. in 1984 at NTT, Japan (Kinoshita et al., 1989). He joined our laboratory in 1995 and has since been actively developing EUVL technology using our synchrotron facility NewSUBARU. Today, EUVL is one of the major themes studied at our laboratory.

To use EUVL in industry, however, a small and strong light source instead of a synchrotron is required. Our group began developing laser-produced plasma (LPP) sources for EUVL in the mid-1990s (Amano et al., 1997). LPP radiation from high-density, high-temperature plasma, which is achieved by illuminating a target with high-peak-power laser irradiation, constitutes an attractive, high-brightness point source for producing radiation from EUV light to x-rays.

Light at a wavelength of 13.5 nm with 2% bandwidth is required for the EUV light source, which is limited by the reflectivity of Mo/Si mirrors in a projection lithography system. Xe and Sn are known well as plasma targets with strong emission around 13.5 nm. Xe was mainly studied initially because of the *debris problem*, in which debris emitted from plasma with EUV light damages mirrors near the plasma, quickly degrading their reflectivity. This problem was of particular concern in the case of a metal target such as Sn because the metal would deposit and remain on the mirrors. On the other hand, Xe is an inert gas and does not deposit on mirrors, and thus has been studied as a deposition-free target. Because of this advantage, researchers initially studied Xe. To provide a continuous supply of Xe at the laser focal point, several possible approaches have been investigated: employing a Xe gas puff target (Fiedrowicz et al., 1999), Xe cluster jet (Kubiak et al., 1996), Xe liquid jet (Anderson et al., 2004; Hansson et al., 2004), Xe capillary jet (Inoue et al., 2007), stream of liquid Xe droplets (Soumagne et al., 2005), and solid Xe pellets (Kubiak et al., 1995). Here, there are solid and liquid states, and their cryogenic Xe targets were expected to provide higher laser-to-EUV power conversion efficiency (CE) owing to their higher density compared with the gas state. In addition, a smaller gas load to be evacuated by the exhaust pump system was expected.

We have also studied a cryogenic Xe solid target. In that study, we measured the EUV emission spectrum in detail, and we found and first reported that the emission peak of Xe was at 10.8 nm, not 13 nm (Shimoura et al., 1998). This meant we could only use the tail of the Xe plasma emission spectrum, not its peak, as the radiation at 13.5 nm wavelength with 2% bandwidth. From this, improvements in the CE at 13.5 nm with 2% bandwidth became a most critical issue for the Xe plasma source; such improvements were necessary to reduce the pumped laser power and cost of the whole EUV light source. On the other hand, the emission peak of a Sn target is at 13.5 nm; therefore, Sn intrinsically has a high CE at 13.5 nm with 2% bandwidth. The CE for Sn is thus higher than that for Xe at present, in spite of our efforts to improve the CE for Xe. This resulted in a trend of using Sn rather than Xe in spite of the debris problem. Today, Cymer (Brandt et al., 2010) and Gigaphoton (Mizoguti et al., 2010), the world's leading manufacturers of LPP-EUV sources, are developing sources using Sn targets pumped with CO_2 lasers while making efforts to mitigate the effects of debris.
In the historical background mentioned above, we developed an LPP-EUV source composed of 1) a fast-rotating cryogenic drum system that can continuously supply a solid Xe target and 2) a high-repetition-rate pulse Nd:YAG slab laser. We have developed the source in terms of its engineering and investigated potential improvements in the CE at 13.5 nm with 2% bandwidth. The CE depends on spatial and temporal Xe plasma conditions (e.g., density, temperature, and size). To achieve a high CE, we controlled the condition parameters and attempted to optimize them by changing the pumping laser conditions. We initially focused on parameters at the wavelength of 13.5 nm with 2% bandwidth required for an EUV lithography source, but the original emission from the Xe plasma has a broad spectrum at 5–17 nm. We noted that this broad source would be highly efficient and very useful for many other applications, if not limiting for EUVL. Therefore, we estimated our source in the wavelength of 5–17 nm. Though Xe is a deposition-free target, there may be sputtering due to the plasma debris. We therefore investigated the plasma debris emitted from our LPP source, which consists of fast ions, fast neutrals, and ice fragments. To mitigate the sputtering, we are investigating the use of Ar buffer gas. In this chapter, we report on the status of our LPP-EUV source and discuss its possibilities.

2. Target system – Rotating cryogenic drum

We considered using a cryogenic solid state Xe target and developed a rotating drum system to supply it continuously, as shown in Fig. 1 (Fukugaki et al., 2006). A cylindrical drum is filled with liquid nitrogen, and the copper surface is thereby cooled to the temperature of liquid nitrogen. Xe gas blown onto the surface condenses to form a solid Xe layer. The drum coated with a solid Xe layer rotates around the vertical z-axis and moves up and down along the z-axis during rotation, moving spirally so that a fresh target surface is supplied continuously for every laser shot. A container wall surrounds the drum surface, except for an area around the laser focus point. This maintains a relatively high-density Xe gas in the gap between the container wall and the drum surface so as to achieve a high growth rate of the layer and fast recovery of the laser craters during rotation. The container wall also suppresses Xe gas leakage to the vacuum chamber to less than 5%, and the vacuum pressure inside the chamber is kept at less than 0.5 Pa. The diameter of the drum is 10 cm. Its mechanical rotation and up–down speed are tunable at 0–1200 rpm and 0–10 mm/s in a range of 3 cm respectively.

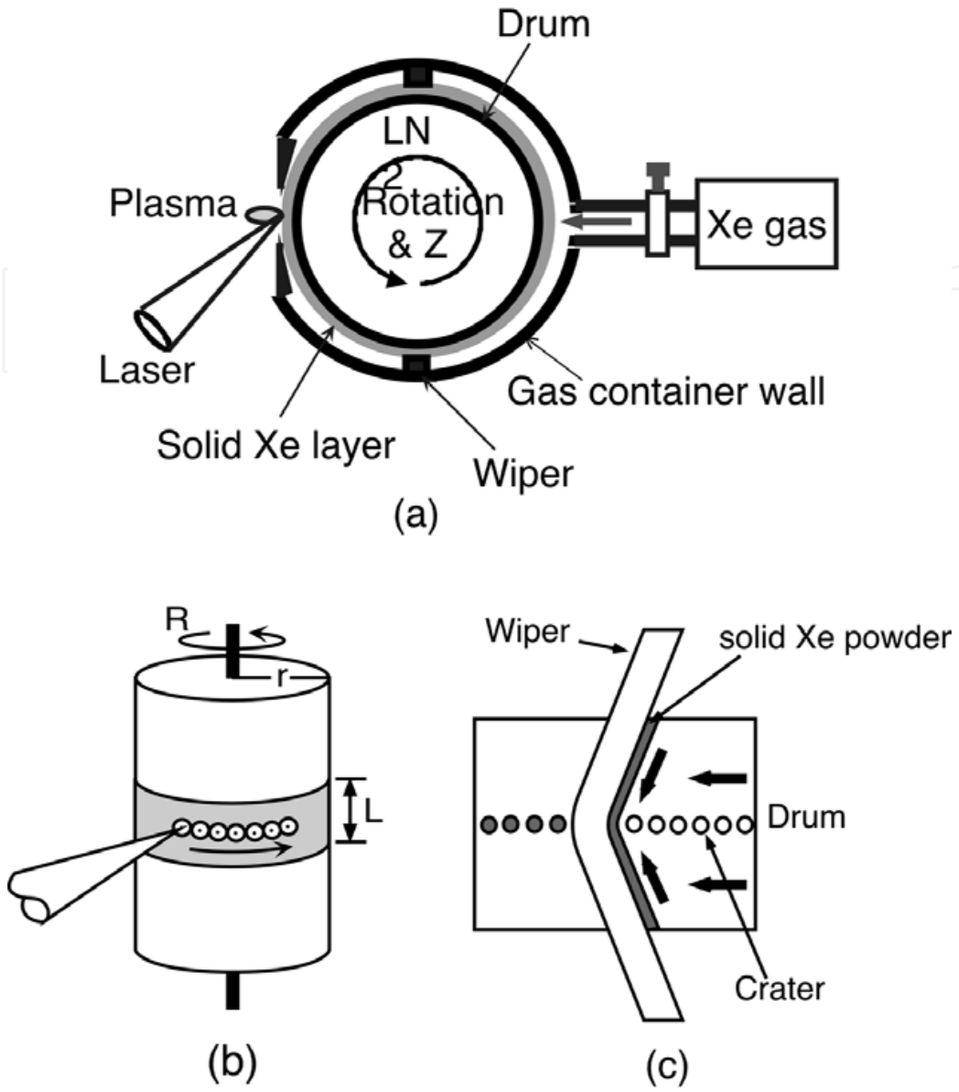

Fig. 1. Illustration of (a) the top view of the rotating cryogenic drum, (b) the side view, and (c) the wiper.

First, we formed a solid Xe layer with thickness of 300–500 μm on the drum surface and measured the size of the laser crater, which depends on the laser pulse energy. The crater diameter was measured directly from a microscope image, and its depth was roughly estimated from the number of shots needed to burn through the known thickness of the layer. A Q-switched 1064 nm Nd:YAG laser was focused on the Xe target surface with a spot diameter of 90 μm. Measured crater diameters D_c and crater depths δ_c are plotted in Fig. 2 for a laser energy range of 0.04–0.7 J. From the results in Fig. 2, a thickness of more than 200 μm was found to be sufficient for a laser shot of 1 J not to damage the drum surface. We then decided the target thickness to be 500 μm.

Two wipers are mounted on the container wall as shown in Fig.1 (a) to adjust the thickness of the solid Xe layer to 500 μm. As shown in Fig. 1 (c), the V-figure wipers also collect the Xe target powder on the craters produced by laser irradiation, thereby increasing the recovery

speed. The wipers demonstrated a recovery speed of 150 μm/s up to a rotation speed of 1000 rpm, at a Xe flow rate of 400 mL/min.

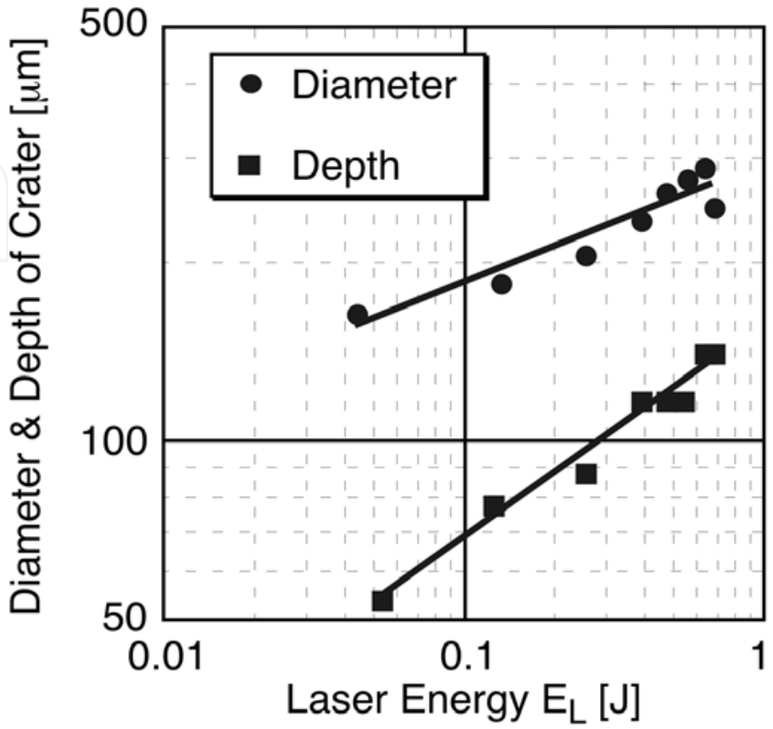

Fig. 2. Measured diameter and depth of a crater as a function of the irradiating laser energy.

Next, operational parameters of the drum are discussed to achieve high-repetition-rate laser pulse irradiation. In Fig. 1(b), R is the rotation speed, r is the radius of the drum, and L is the range of motion (scanning width of the target) along the rotational axis (z-axis). When the laser pulses are irradiated with frequency f, craters form on the target with separation length d between adjacent craters. The recovery time of a crater is T. Under the condition that craters do not overlap, f and T can be written as

$$f = \frac{2\pi r \cdot R}{d} \tag{1}$$

$$T = \frac{2\pi rL}{f \cdot d^2} \tag{2}$$

For example, if we assume laser energy of E_L = 1 J, a formed crater has a diameter of D_c = 300 μm and a depth of δ_c = 160 μm, and d must be at least 300 μm for the craters not to overlap. At r = 5 cm and R = 1000 rpm, we obtain f = 17 kHz from Eq. (1). When f = 10 kHz and L = 3 cm, T is calculated to be 10 s using Eq. (2), and we know that a recovery speed of the crater ($V_c = \delta_c / T$) of 16 μm/s is required. Here, we have already obtained V_c = 150 μm/s via the wiper effect and the required speed has been achieved.

Although flaking of the target layer due to superimposition of shock and/or thermal waves produced by continuous laser pulses was a concern for high-repetition pulse operation, model experiments and calculations show that there is no problem up to 1 J per pulse and 10 kHz (Inoue et al., 2006).
From the above results, we conclude that the rotating drum system we developed can supply the target continuously, achieving the required laser irradiation of 10 kHz and 1 J, and thus realizing a high-average-power EUV light source.

3. Drive laser – Nd:YAG slab laser

High peak power and high focusability (i.e., high beam quality) are required for a driving laser to produce plasma. In addition, high average power is required for high throughput in industrial use such as EUVL. We express such a laser as a *high average and high peak brightness laser*, for which the average brightness and peak brightness are defined as average power/$(\lambda \cdot M^2)^2$ and peak power/$(\lambda \cdot M^2)^2$, respectively; we began studying such lasers in the 1990s (Amano et al, 1997,1999).
We attempted to realize a *high average and high peak brightness laser* using a solid-state Nd:YAG laser (Amano et al., 2001). The thermal-lens effect and thermally induced birefringence in an active medium are serious for such a laser; thus, thermal management of the amplifier head is more critical, and the design of the amplifier system must more efficiently extract energy and more accurately correct the remaining thermally induced wavefront aberrations in the pumping head. To meet these requirements, we developed a phase-conjugated master-oscillator-power-amplifier (PC-MOPA) Nd:YAG laser system consisting of a diode-pumped master oscillator and flash-lamp-pumped angular-multiplexing slab power-amplifier geometry incorporating a stimulated-Brillouin-scattering phase-conjugate mirror (SBS-PCM) and image relays (IR). The system design and a photograph are shown in Fig. 3. This laser demonstrated simultaneous maximum average power of 235 W and maximum peak power of 30 MW with $M^2 = 1.5$. The maximum pulse energy was 0.73 J with pulse duration of 24 ns at a pulse repetition rate of 320 pps. We therefore obtained, simultaneously, both high average brightness of 7×10^9 W/cm^2·sr and high peak brightness of 1×10^{15} W/cm^2·sr.
This peak brightness is enough to produce plasma but the average brightness needs to be higher for EUVL applications. The maximum average power is mainly limited by the thermal load caused by flash-lamp-pumping in amplifiers. The system design rules that we confirmed predicted that average output power at the kilowatt level can be achieved by replacing lamp pumping in the amplifier with laser-diode pumping. Since our work, it seems that there has been no major progress in laser engineering for such *high average and high peak brightness lasers*. Average power of more than 10 kW has been achieved in continuous-wave solid-state lasers using configurations of fibers (ex. IPG Photonics Corp.) or thin discs (ex. TRUMPF GmbH). On the other hand, for the short-pulse lasers mentioned above, the maximum average power remains around 1 kW (Soumagne et al., 2005), which is more than an order of magnitude less than the ~30 kW required for an industrial EUVL source. This is one of the reasons why CO_2 lasers have been preferred over Nd:YAG lasers as the driving laser. To further the industrial use of solid-state lasers, there needs to be a breakthrough to increase the average power.

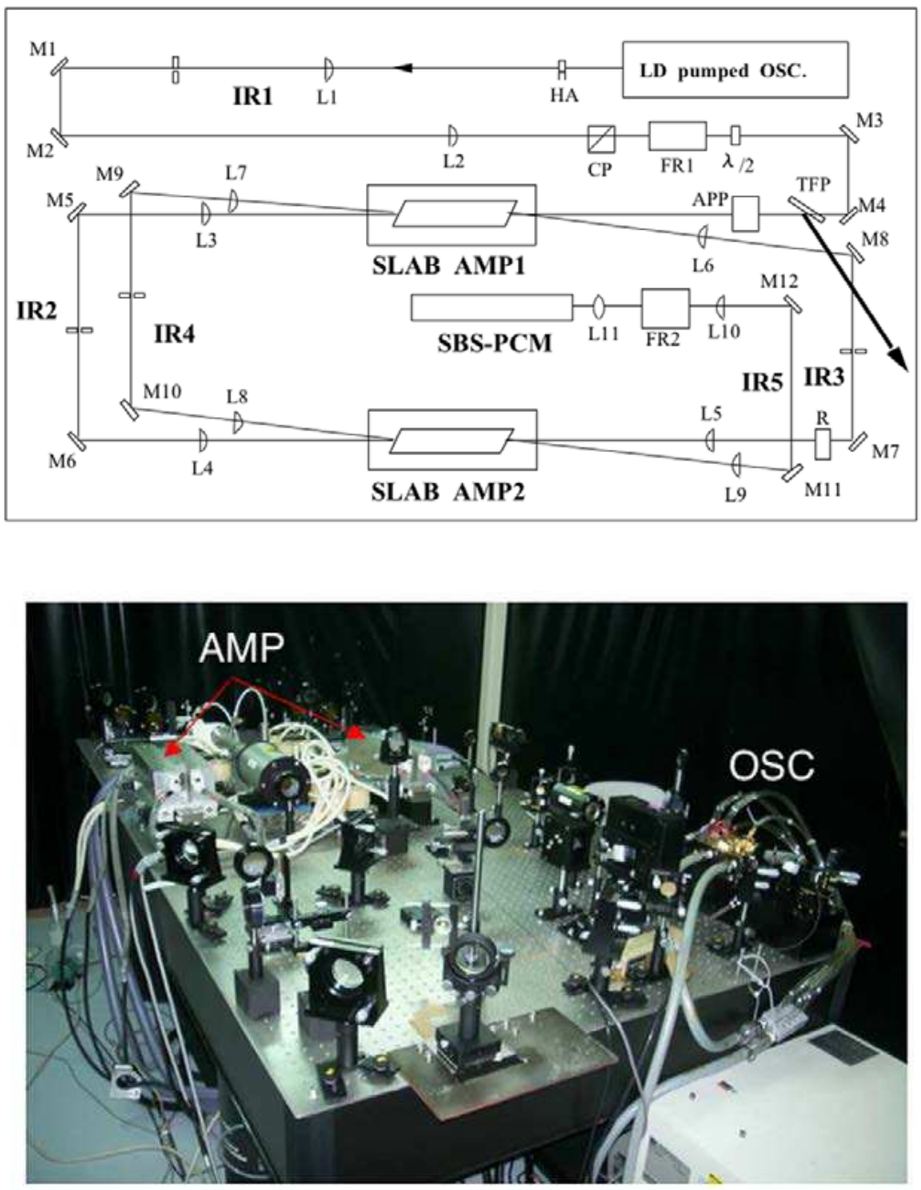

Fig. 3. Experimental setup and photograph of the PC-MOPA laser system.

4. EUV source

Figure 4 is an illustration and a photograph of the LPP-EUV source composed of a rotating cryogenic drum and Nd:YAG slab laser. The drum, detectors, and irradiating samples are installed in a vacuum chamber because EUV light cannot transmit through air. Driving laser pulses passing through the window are focused perpendicularly on the target by the lens so that Xe plasma is produced and EUV radiation is emitted. At a repetition rate of 320 Hz and average power of 110 W, the laser pulses irradiate the Xe solid target on the rotating drum with laser intensity of ~10^{10} W/cm^2. The rotation speed is 130 rpm and the vertical speed 3

mm/s. The Xe target gas is continuously supplied at a flow rate of 400 mL/min. Under these operation conditions, we obtain continuous EUV generation with average power of 1 W at 13.5 nm and 2% bandwidth.

The driving pulse energy was determined to be 0.3 J under the optimal condition that higher CE and lower debris are simultaneously achieved, as detailed below. At present, the maximum achieved CE is 0.9% at 13.5 nm with 2% bandwidth for the optimal condition. Under drum-rotating operation, we found the good characteristics of increased CE and less fast ions compared with the case with the drum at rest. We next detail the EUV and debris characteristics of the EUV source.

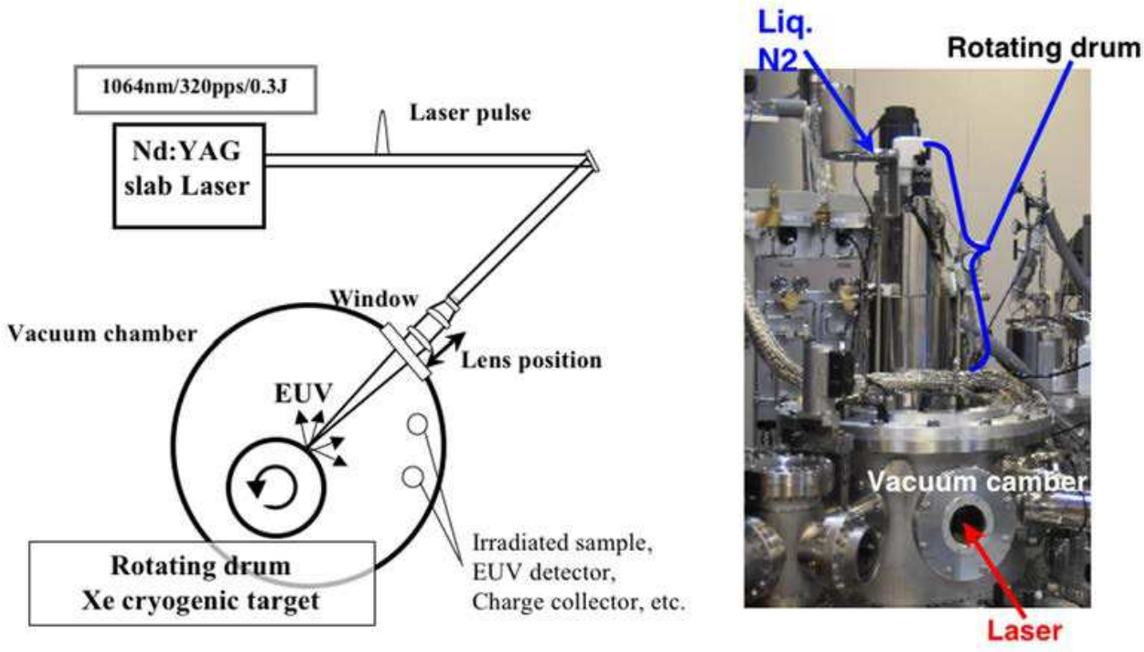

Fig. 4. Experimental setup and photograph of the laser plasma EUV source.

5. Conversion efficiency for EUVL

In this section, we report our studies carried out to improve the CE at 13.5 nm with 2% bandwidth required for the EUVL source (Amano et al., 2008, 2010a). To achieve the highest CE, we attempted to control the plasma parameter by changing the driving laser conditions. We investigated dependences of the CE on the drum rotation speed, laser energy, and laser wavelength. We also carried out double-pulse irradiation experiments to improve the CE.

To obtain data of EUV emission, a conventional Q-switched Nd:YAG rod laser (Spectra-Physics, PRO-230) was used in single-shot operation. By changing the position of the focusing lens to change the laser spot, the laser intensity on the target was adjusted to find the optimum intensity. We note that the lens position (LP) is zero at best focus, negative for in-focus (the laser spot in the target before the focus) and positive for out-of-focus (beyond the focus).

Figure 5(a) shows the CE per solid angle as a function of LP (laser intensity), which was measured by an EUV energy detector calibrated absolutely—*Flying Circus* (SCIENTEC Engineering)—located 45 degrees from the laser incident axis. The laser pulse energy was 0.8 J. We see that the CE was higher under the rotating-drum condition than under the rest condition. Here, the rest condition is as follows. Xe gas flow is stopped (0 mL/min) after the target layer has formed, and the drum rests (0 rpm) during a laser shot and stepwise rotates after every shot so that a fresh target is supplied to the point irradiated by the laser. The rotation condition is as follows. Laser pulses irradiate quasi-continuously the target on the rotating drum (>3 rpm), supplying Xe gas (>40 mL/min) and forming the target layer. The EUV intensity increased immediately with slow rotation (>3 rpm) and appeared to be almost independent of the rotation speed. In Fig. 5(a), we see that the maximum CE per solid angle was for an optimized laser intensity of 1×10^{10} W/cm^2 (LP = –10 mm) during rotation. The EUV angular distribution could be expressed by a fitting curve of $(\cos\theta)^{0.38}$, and taking into account this distribution, we obtained the maximum spatially integrated CE of 0.9% at 13.5 nm with 2% bandwidth. EUV spectra at laser intensity of 1×10^{10} W/cm^2 are shown in Fig. 5(b). It is obvious that the emission of the 13.5 nm band was greater in the case of rotation than it was in the case of rest.

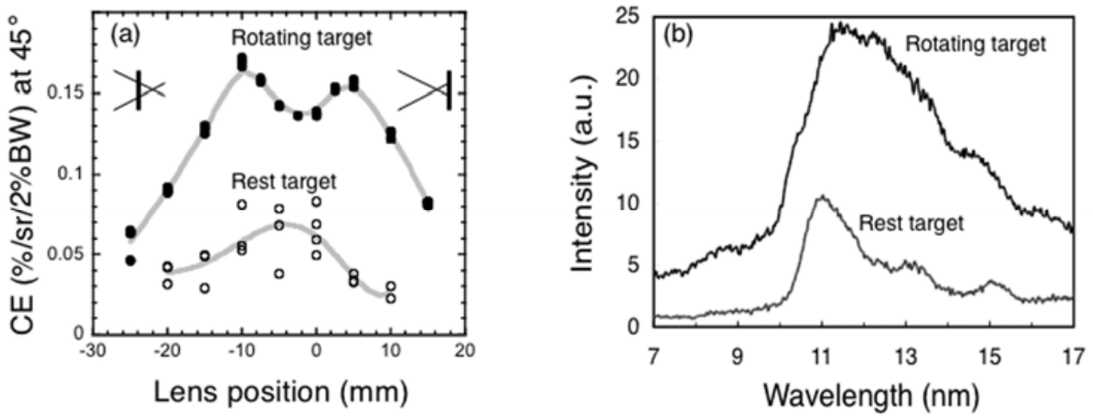

Fig. 5. (a) CE at the wavelength of 13.5 nm with 2% bandwidth as a function of LP under the rotation (130 rpm) and at-rest (0 rpm) conditions. The laser energy was 0.8 J. Insets show the laser beam focusing on the target. (b) Spectra of EUV radiation from the cryogenic Xe drum targets under the rotation (bold line) and at-rest (narrow line) conditions with laser intensity of 1×10^{10} W/cm^2 for LP of –10 mm.

We considered the mechanism for the increase in EUV intensity with rotation of the target. Figure 6 shows photographs of the visible emission from the Xe target observed from a transverse direction. It shows an obvious expansion of the emitting area with longer (optically thicker) plasma in the rotating case compared with the at-rest case. These images indicate the existence of any gas on the target surface. Under the rotation condition, Xe gas is supplied continuously to grow the target layer and the wipers form the layer. However, the wipers are not chilled especially, and the temperature of the target surface might increase owing to contact with the wipers in the rotating case so that the vapor pressure

increases. Therefore, the vaporized Xe gas from the target surface was considered as the gas on the target. Although additional Xe gas was added from outside the vacuum chamber, the EUV intensity did not increase and in fact decreased owing to gas absorption. Therefore, it is supposed that Xe gas with adequate pressure localizes only near the target surface. From these results, we conclude that Xe gas on the target surface in the rotating drum produces optically thick plasma that has optimized density and temperature for emitting EUV radiation, and satellite lines of the plasma contribute effectively to increasing the EUV intensity (Sasaki et al., 2004).

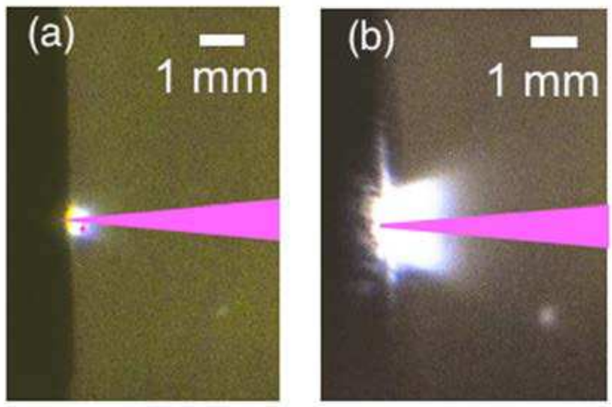

Fig. 6. Images of visible emissions from the plasma on the resting (a) and rotating (b) targets.

Next, the dependence of the laser pulse energy was investigated. We measured the CE as a function of laser energy at different LPs in the rotating drum. For laser energies exceeding 0.3 J, a CE of nearly 0.9% was achieved by tuning the LP with the laser intensity optimized as ~10^{10} W/cm^2. In the energy range, the maximum CE did not depend on the laser energy. At the LP in this experiment, the spot size on the target was larger than 500 μm and plasma energy loss at the edges could be ignored for this large spot. Therefore, the same CE was achieved at the same laser intensity. However, in the lower energy region, the spot size must be small to achieve optimal laser intensity, and edge loss due to three-dimensional expansion in plasma cannot then be ignored and a decrease in the CE was observed. Therefore, it is concluded that laser energy must exceed 0.3 J to achieve a high CE.

The dependence of the laser wavelength was also investigated. Additionally, we carried out 1 ω double-pulse irradiation experiments in which a pre-pulse produces plasma with optimal density and temperature, and after a time delay, a main laser pulse effectively injects emission energy into the expanded plasma to increase the CE. Under the rest condition, there were increases in CE for the shorter laser or the double pulse irradiation (Miyamoto et al., 2005, 2006). In both cases, the long-scale plasmas and their emission spectra were observed to be similar to those under the rotation condition for 1 ω single-pulse irradiation. Therefore, we supposed that in the both cases, the CE was increased by the same mechanism described above. However, when the shorter pulses or the double pulses were emitted under the rotating condition, the CE did not increase but decreased. It is considered that the opacity of the plasma was too great in these experiments and the best condition was not achieved.

In conclusion, the maximum CE was found to be 0.9% at 13.5 nm with 2% bandwidth for the optimal condition.

6. Xe plasma debris

In this section, we report the characteristics of the plasma debris that damages mirrors (Amano et al., 2010b). First, we investigated fast ions, fast neutrals and ice fragments, which constitute the debris.

When we found that EUV radiation was greater for a rotating drum than for a drum at rest, we also found that the number of fast ions decreased simultaneously. Figure 7(a) shows ion signals from a charge collector (CC) with laser pulse energy of 0.5 J and optimal intensity of 10^{10} W/cm^2, for different drum rotation speeds. The ion signal reduces rapidly after the drum starts to rotate (> 4 rpm), after which the signal is almost independent of rotation speed. Ion energy spectra were obtained as shown in Fig. 7(b) using the time-of-flight signals shown in Fig. 7(a). Here, we assume that all ions were doubly charged because we measured the principle charge state of Xe ions to be two with an electrostatic energy analyzer (Inoue et al., 2005). Under the rotation condition, the maximum ion energy decreases to 6 keV and the number of high-energy ions (with energy of a few dozen kilo-electron-volts) also decreases. These are favorable characteristics for the debris problem. The decrease in the ion count under the rotation condition can be explained by a *gas curtain effect* that originates from the Xe gas localized at the target surface. The pressure of this localized Xe gas can be roughly estimated from the peak attenuation (η) in Fig. 7(a); we estimated the product of pressure and thickness to be about 10 Pa·mm.

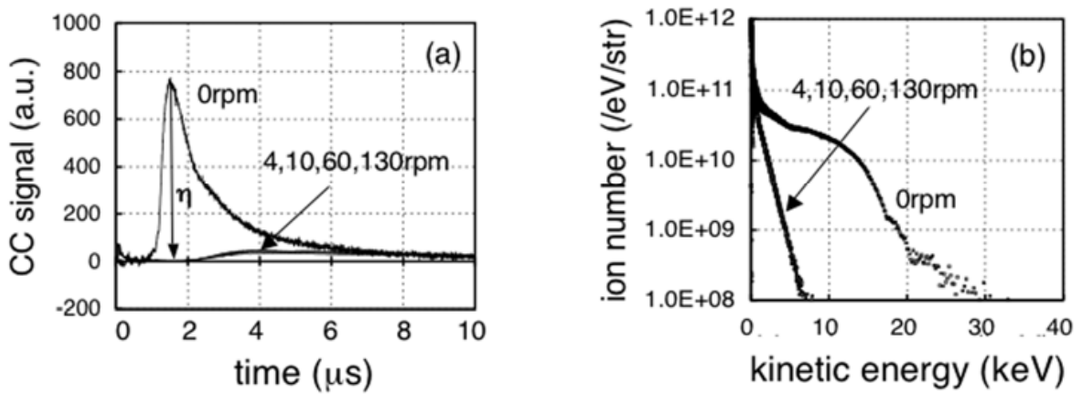

Fig. 7. (a) CC signals of ions and (b) their energy spectra at rotation speeds of 0, 4, 10, 60 and 130 rpm. η in (a) is the loss rate of ions due to the drum rotating. The ion number in (b) was calculated assuming the charge state was two.

Fast neutral particles were measured by the microchannel plate (MCP) detector when the number of fast ions decreased under the rotation condition. The MCP is sensitive to both ions and neutrals, making the use an electric field obligatory to repel ions so that the MCP detects only neutral particles. From the measurement, we found the number of neutrals to be approximately an order of magnitude less than the number of ions.

In the case of solid Xe targets, ice fragments might be produced by shock waves of laser irradiation, whereas this is not the case for gas or liquid targets. In early experiments using a solid Xe pellet, ice fragments were observed and mirror damage due to these fragments was

indicated (Kubiak et al., 1995). Since these reports, liquid Xe targets have been preferred over solid Xe targets, with the exception of our group. It is therefore necessary to clarify characteristics of fragment debris from a solid Xe target on a rotating cryogenic drum. After exposing a Si sample to the Xe plasmas pumped by 100 laser pulses, we observed fragment impact damage on its surface using a scanning electron microscope. We observed damage spots on the samples at laser energy of 0.8 J irrespective of whether the drum rotates. Conversely, we did not observe spots at laser energy of 0.3 J. To explain these results, we consider that the fragment speed (kinetic energy) might drop below a damage threshold upon reducing the laser pulse energy because the fragment speed is a function of incident laser energy (Mochizuki et al., 2001). Observing the damage spots, we know that the fragment size was larger than a few microns, and the gas curtain might not be effective for such large fragments. This would explain why the fragment impact damage was independent of the state of drum rotation. From these results, we conclude that fragment impact damage, which occurs especially for the solid Xe target, can be avoided simply by reducing the incident laser pulse energy to less than 0.3 J.

The laser pulse energy was set to 0.3 J to avoid fragment impact damage and the laser repetition rate was 320 pps, giving an average power of 100 W. Next, we investigated damage to a Mo/Si mirror, which was the result of total plasma debris (mainly fast ions) from the laser multi-shots experiments. After 10 min plasma exposure, the sputtered depth was measured to be 50 nm on the surface of a Mo/Si mirror placed 100 mm from the plasma at a 22.5-degree angle to the incident laser beam. Because a typical Mo/Si mirror has 40 layer pairs and the thickness of one pair is approximately 6.6 nm, all layers will be removed within an hour by the sputtering. Although Xe is a deposition-free target, sputtering by debris needs to be mitigated. However, the major plasma debris component is ions, and we believe their mitigation to be simple compared with the case of a metal target such as Sn, using magnetic/electric fields and/or gas. We are now studying debris mitigation by Ar buffer gas. Ar gas was chosen because of its higher stopping power for Xe ions and lower absorption of EUV light, and its easy handling and low cost. After the vacuum chamber was filled with Ar gas, total erosion rates were measured using a gold-coated quartz crystal microbalance sensor placed 77 mm from the plasma at a 45-degree angle, and simultaneously, EUV losses were monitored by an EUV detector placed 200 mm from the plasma at a 22.5-degree angle. Figure 8 shows the erosion rates as a function of Ar gas pressure. The rates were normalized by the erosion N_0 at a pressure of 0 Pa. When the Ar pressure was 8 Pa, we found the erosion rate was 1/18 of that without the gas, but the absorption loss for EUV light was only 8%. The erosion rates (N/N_0) in Fig. 8 can be fitted to an exponential curve:

$$N\left(P_{Ar}\right) = N_0 \cdot \exp\left(-\frac{P_{Ar}}{kT}\sigma l\right) \tag{3}$$

where P_{Ar} is the Ar pressure, k is the Boltzmann constant, T is the gas temperature, σ is the cross section and l is the debris flight length. From this fitting, we obtain $\sigma = 2.0 \times 10^{-20}$ m^2. The Ar buffer gas successfully mitigated the effect of plasma debris with little EUV attenuation. Increasing the Ar pressure, mirror erosion decreases but EUV attenuation increases. Compromising the erosion and EUV attenuation, an optimized pressure is achieved. We should localize the higher density Ar gas to only the debris path so that EUV attenuation is as small as possible. We can design the optimized pressure condition using

the σ value obtained and we consider the use of an Ar gas jet. Through this mitigation, we expect that erosion will be reduced by more than two orders of magnitude and the lifetime of the mirror will be extended. We believe the debris problem for Xe plasma will thus be solved.

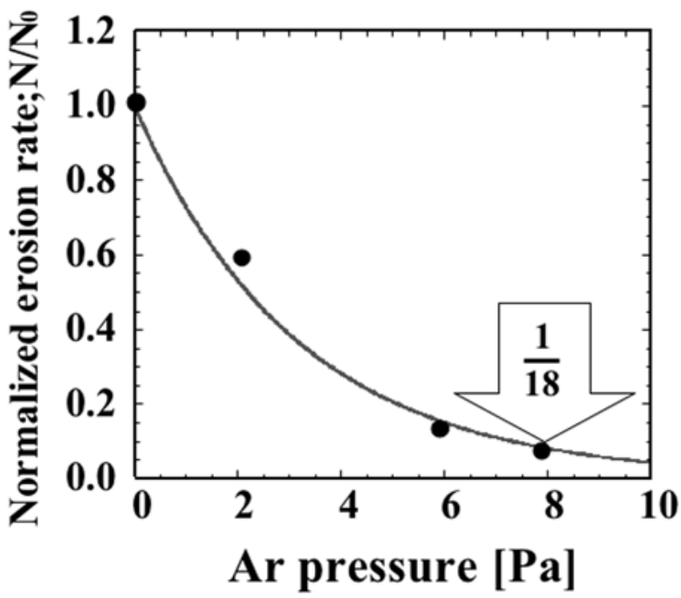

Fig. 8. Normalized erosion rate as a function of Ar pressure. The laser energy was 0.3 J and the rotation speed was 130 rpm.

7. EUV emission at 5-17nm

We began developing the LPP source for EUVL and characterized it at 13.5 nm with 2% bandwidth, but Xe plasma emission has originally a broad continuous spectrum as shown in Fig. 9. If the broad emission is used, our source will be very efficient, not limiting its applications to EUVL. We characterized the source again in the wavelength range of 5–17 nm. Figure 10 shows the CE at 5–17 nm as a function of LP (laser intensity) with laser energy of 0.8 J. The maximum spatially integrated CE at 5–17 nm was 30% for optimal laser intensity of 1×10^{10} W/cm^2. The maximum CE depended on the laser energy and was 21% at 0.3 J. Therefore, high average power of 20 W at 5–17 nm has been achieved for pumping by the slab laser with 100 W (0.3 J at 320 pps). We consider this a powerful and useful source.

Recently, new lithography using La/B_4C mirrors having a reflectivity peak at 6.7 nm was proposed as a next-generation candidate following EUVL using Mo/Si mirrors having a reflectivity peak at 13.5 nm (Benschop, 2009). This means that a light source emitting around 6 nm will be required in a future lithograph for industrial mass production of semiconductors. Because our source emits broadly at 5–17 nm as mentioned above, it can obviously be such a 6 nm light source. We thus next characterized it as a source emitting at 6.7 nm. Here we did not carry out new experiments to optimize the plasma for emitting at 6.7 nm but looked for indications of strong emission at 6.7 nm from the spectrum data

already acquired. When making efforts to improve the CE at 13.5 nm, we noticed that emissions around 6 nm became strong at higher laser intensity. When laser energy is 0.8 J and LP = 0 mm (i.e., laser intensity is 4×10^{12} W/cm^2 under the rotation condition), there is a hump around 6 nm as shown in Fig. 9. The spatially integrated CE at 6.7 nm with 0.6% bandwidth is estimated to be 0.1% from this spectrum. Because the bandwidth of 0.6% for the La/B_4C mirror reflectivity is narrower than the 2% for the Mo/Si mirror, the available reflected power is intrinsically small. The CE of 0.1% was not obtained under optimized conditions and higher CE may be achieved in the future. In any event, our source is only one LPP source at present that can generate continuously an emission at 6.7 nm.

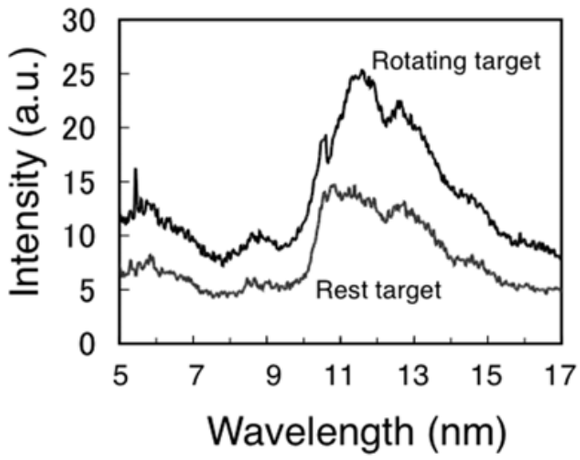

Fig. 9. Spectra of EUV radiation under the rotation (bold line) and at-rest (narrow line) conditions with laser intensity of 4×10^{12}W/cm^2 for best focus (LP = 0 mm). The laser energy was 0.8 J.

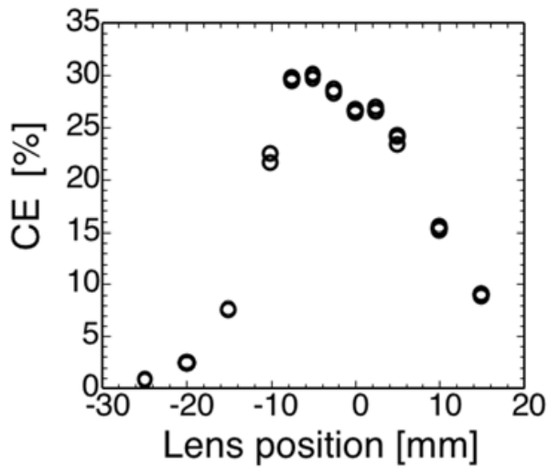

Fig. 10. CE for a wavelength of 5–17 nm as a function of LP under the rotation (130 rpm) condition. The laser energy was 0.8 J.

8. Conclusion

This chapter briefly reviewed our LPP-EUV source. First, we characterized the source at a wavelength of 13.5 nm with 2% bandwidth as an EUVL source and achieved a maximum CE of 0.9%. When the driving laser power is 110 W at 320 pps, the average power of 1 W is obtained at the wavelength and this is thought to be sufficient for the source to be used in various studies. However, the EUV power required for industrial semiconductor products is more than 100 W at present; our power is two orders of magnitude less. To approach the requirements of an industrial EUV source, the remaining tasks are considered. The majority of Xe plasma debris is fast ions, which can be mitigated using gas and/or a magnetic/electric field relatively easily. The drum system can supply the Xe target for laser pulses with energy up to 1 J at 10 kHz. Therefore, a remaining task is powering up the driving laser. A short pulse laser with average power of the order of 10 kW (i.e., *high average and high peak brightness laser*) must be developed and such a breakthrough is much hoped for.

Not limiting the wavelength to 13.5 nm with 2% bandwidth and using the broad emission at 5–17 nm, a maximum CE of 30% is achieved. Pumping with laser power of 100 W, high average power of 20 W is already obtained and the source is useful for applications other than industrial EUVL using Mo/Si mirrors. We are now applying our source to microprocessing and/or material surface modification. Our source also emits around the wavelength of 6 nm considered desirable for the next lithography source. In conclusion, our LPP source is a practicable continuous EUV source having possibilities for various applications.

9. Acknowledgment

Part of this work was performed under the auspices of MEXT (Ministry of Education, Culture, Sports, Science and Technology, Japan) under the contract subject "Leading Project for EUV lithography source development".

10. References

Amano, S., Shimoura, A., Miyamoto, S. & Mochizuki, T. (1997). High-repetition-rate pulse Nd:YAG slab laser for x-ray source by cryogenic target, *1997 OSA Technical Digest Series, Vol.11, Conference Edition, CLEO97,* p.523, Baltimore, USA, May 18-23, 1997

Amano, S., Shimoura, A., Miyamoto, S. & Mochizuki, T. (1999). Development of a high repetition rate Nd:YAG slab laser and soft X-ray generation by X-ray cryogenic target. *Fusion Eng. and Design* 44, pp.423-426

Amano, S. & Mochizuki, T. (2001). High average and high peak brightness slab laser. *IEEE J. Quantum Electron.* 37(2), pp.296-303

Amano, S., Nagano, A.: Inoue, T., Miyamoto, S. & Mochizuki, T. (2008). EUV light sources by laser-produced plasmas using cryogenic Xe and Li targets. *Rev. Laser. Eng.* 36(11), pp.715-720 (in Japanese)

Amano, S., Masuda, K., Shimoura, A., Miyamoto, S. & Mochizuki, T. (2010a). Characterization of a laser-plasma extreme ultraviolet source using a rotating cryogenic Xe target. *Appl. Phys.B* 101, pp.213-219

Amano, S., Inaoka, Y., Hiraishi, H., Miyamoto, S. & Mochizuki, T. (2010b). Laser-plasma debris from a rotating cryogenic-solid-Xe target. *Rev. Sci. Instrum.* 81, pp. 023104-1-023104-6

Anderson, R.J., Buchenauer, D.A., Klebanoff, L., Wood II, O.R. & Edwards, N.V. (2004). The erosion of materials exposed to a laser-pulsed plasma (LPP) extreme ultraviolet (EUV) illumination source, *Proceedings of SPIE, Emerging Lithographic Technologies VIII*, vol.5374, pp.710-719, Santa Clara, USA, February 2004

Bakshi,V.(Ed). (2005) *EUV Sources for Lithography*, SPIE, ISBN:0819458457, Bellingham, WA

Benschop, J. (2009). EUV: past, present and prospects, Keynote I, *2009 International Symposium on Extreme Ultraviolet Lithography*, Prague Czech, October 2009, International Sematech, Available from: <http://www.sematech.org/meetings/archives/litho/index.htm>

Brandt, D.C., Fomenkov, I.V., Partlo, W.N., Myers, D.W., Kwestens, P., Ershov, A.I., Bowering, N.R., Baumgart, P., Bykanov, A.N., Vaschenko, G.O., Khodykin, O.V., Srivastava, S., Hou, R., Dea, S.D., Ahmad, I. & Rajyuguru, C. (2010). LPP EUV source production for HVM, SO-01, *2010 International Symposium on Extreme Ultraviolet Lithography*, Kobe Japan, October 2010, International Sematech, Available from: <http://www.sematech.org/meetings/archives/litho/index.htm>

Fiedorowicz, H., Bartnik, A., Szczurek, M., Daido, H., Sakaya. N., Kmetik, V., Kato, Y., Suzuki, M., Matsumura, M., Yajima, J., Nakayma, T. & Wilhein, T. (1999). Investigation of soft X-ray emission from a gas puff target irradiated with a Nd:YAG laser, *Opt.Comm.*,163(1-3), pp.103-114

Fukugaki, K., Amano, S., Shimoura, A., Inoue, T., Miyamoto, S. & Mochizuki, T. (2006). Rotating cryogenic drum supplying Xe target to generate extreme ultraviolet radiation. *Rev. Sci. Instrum.* 77, pp.063114-1-063114-4

Hansson, B.A.M., Hemberg, O., Hertz, M.H., Berglund, M., Choi, H. J., Jacobsson, B., Janin, E., Mosesson, S., Rymell, L., Thoresen, J. & Wilner, M. (2004). Characterization of a liquid-xenon-jet laser-plasma extreme-ultraviolet source. *Rev.Sci.Instrum.* 75(6), pp.2122-2129

Inoue, T., Kaku, K., Shimoura, A., Nica, P.E., Sekioka, T., Amano, S., Miyamoto, S. & Mochizuki, T. (2005). Studies on laser-produced plasma EUV generation by using fast-supplyunig cryogenic Xe targets, 1-SO-10, *2005 International Symposium on Extreme Ultraviolet Lithography*, San Diego, USA, November 2005, International Sematech, Available from: <http://www.sematech.org/meetings/archives/litho/index.htm>

Inoue, T., Amano, S., Miyamoto, S. & Mochizuki, T. (2006). The stability of a rotating-drum solid-Xe target subjected to high-repetition rate laser irradiation for laser-plasma EUV generation. *Rev. Laser. Eng.* 34(8), pp.570-574 (in Japanese)

Inoue, T., Okino, H., Nica, P.E., Amano, S., Miyamoto, S. & Mochizuki, T. (2007). Xe capillary target for laser-plasma extreme ultraviolet source. *Rev. Sci. Instrum.* 78, pp.105105-1-105105-5

Kinoshita, H., Kurihara, K., Ishii,Y. & Torii, Y. (1989). Soft x-ray reduction lithography using multilayer mirrors. *J. Vac. Sci. Technol.B*, 7(6), pp.1648-1651

Kubiak, G., Krentz. K., Berger, K., Trucano, T., Fisher, P. & Gouge, M. (1995). Cryogenic pellet laser plasma source targets, *OSA Proceedings on Soft X-ray Projection Lithography*, vol.23, pp.248-254, Monterey, USA, September 1994

Kubiak, G., Bernardez, L.J., Krenz, K.D., O'Connell, D.J., Gutowski, R. & Todd, A.M., (1996). Debris-free EUVL sources based on gas jets, *OSA TOPS on Extreme Ultraviolet Lithography*, vol.4, pp.66-71

Miyamoto, S., Shimoura, A., Amano, S., Fukugaki, K., Kinugasa, H., Inoue, T. & Mochizuki, T. (2005). Laser wavelength and spot diameter dependence of extreme ultraviolet conversion efficiency in ω, 2ω, and 3ω Nd:YAG laser-produced plasmas. *Appl. Phys. Lett.* 86(26), pp.261502-1-261502-3

Miyamoto, S., Amano, S.: Inoue, T., Nica, P. E., Shimoura, A., Kaku, K., Sekioka, T. & Mochizuki, T. (2006). EUV source developments on laser-produced plasmas using cryogenic Xe and Lithium new scheme target, *Proceedings of SPIE, Emerging Lithographic Technologies X*, vol.6151, pp.61513S-1-61513S-10, San Jose, USA, February 2006

Mizoguti, H., Abe, T., Watanabe, Y., Ishihara, T., Ohta, T., Hori, T., Kurosu, A., Komori, H., Kakizaki, K., Sumitani, A., Wakabayashi, O., Nakarai, H., Fujimoto, J. & Endo, A. (2010). 1st generation laser-produced plasma 100W source system for HVM EUV lithography, SO-03, *2010 International Symposium on Extreme Ultraviolet Lithography*, Kobe Japan, October 2010, International Sematech, Available from: <http://www.sematech.org/meetings/archives/litho/index.htm>

Mochizuki, T., Shimoura, A., Amano, S. & Miyamoto, S. (2001). Compact high-average-power X-ray source by cryogenic target, *Proceedings of SPIE, Applications of X Rays Generated from Lasers and Other Bright Sources II*, vol.4504, pp.87-96, San Diego, USA, July 2001

Sasaki, A., Nishihara, K., Murakami, M., Koike, F., Kagawa, T., Nishikawa, T., Fujima, K., Kawamura, T. & Furukawa, H. (2004). Effect of the satellite lines and opacity on the extreme ultraviolet emission from high-density Xe plasmas. *Appl. Phys. Lett.* 85(24), pp.5857-5859

Shimoura, A., Amano, S., Miyamoto, S. & Mochizuki, T. (1998). X-ray generation in cryogenic targets irradiated by 1 μm pulse laser. *Appl. Phys. Lett.* 72(2), pp.164-166

Soumagne, G.: Abe, T., Suganuma,T. , Imai, Y., Someya, H., Hoshino, H., Nakano, M., Komori, H., Takabayashi, Y., Ariga, T., Ueno, Y., Wada, Y., Endo, A & Toyoda, K.(2005). Laser-produced-plasma light source for EUV lithography, *Proceedings of SPIE, Emerging Lithographic Technologies IX*, vol.5751, pp.822-828, San Jose, USA, March 2005

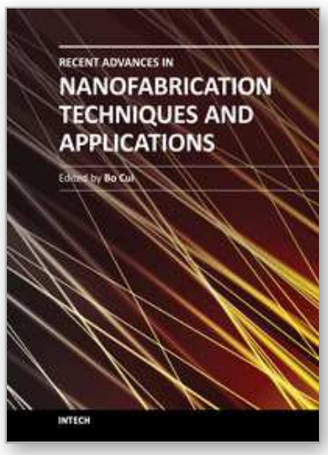

Recent Advances in Nanofabrication Techniques and Applications
Edited by Prof. Bo Cui

ISBN 978-953-307-602-7
Hard cover, 614 pages
Publisher InTech
Published online 02, December, 2011
Published in print edition December, 2011

Nanotechnology has experienced a rapid growth in the past decade, largely owing to the rapid advances in nanofabrication techniques employed to fabricate nano-devices. Nanofabrication can be divided into two categories: "bottom up" approach using chemical synthesis or self assembly, and "top down" approach using nanolithography, thin film deposition and etching techniques. Both topics are covered, though with a focus on the second category. This book contains twenty nine chapters and aims to provide the fundamentals and recent advances of nanofabrication techniques, as well as its device applications. Most chapters focus on in-depth studies of a particular research field, and are thus targeted for researchers, though some chapters focus on the basics of lithographic techniques accessible for upper year undergraduate students. Divided into five parts, this book covers electron beam, focused ion beam, nanoimprint, deep and extreme UV, X-ray, scanning probe, interference, two-photon, and nanosphere lithography.

How to reference
In order to correctly reference this scholarly work, feel free to copy and paste the following:

Sho Amano (2011). Laser-Plasma Extreme Ultraviolet Source Incorporating a Cryogenic Xe Target, Recent Advances in Nanofabrication Techniques and Applications, Prof. Bo Cui (Ed.), ISBN: 978-953-307-602-7, InTech, Available from: http://www.intechopen.com/books/recent-advances-in-nanofabrication-techniques-and-applications/laser-plasma-extreme-ultraviolet-source-incorporating-a-cryogenic-xe-target

INTECH
open science | open minds

InTech Europe
University Campus STeP Ri
Slavka Krautzeka 83/A
51000 Rijeka, Croatia
Phone: +385 (51) 770 447
Fax: +385 (51) 686 166
www.intechopen.com

InTech China
Unit 405, Office Block, Hotel Equatorial Shanghai
No.65, Yan An Road (West), Shanghai, 200040, China
中国上海市延安西路65号上海国际贵都大饭店办公楼405单元
Phone: +86-21-62489820
Fax: +86-21-62489821

IntechOpen